Particle-in-cell simulations of the magnetoacoustic cyclotron instability of fusion-born alpha-particles in tokamak plasmas

2013 Plasma Phys. Control. Fusion 55 065003

(http://iopscience.iop.org/0741-3335/55/6/065003)

Plasma Phys. Control. Fusion **55** (2013) 065003 (6pp) doi:10.1088/0741-3335/55/6/065003

Particle-in-cell simulations of the magnetoacoustic cyclotron instability of fusion-born alpha-particles in tokamak plasmas

J W S Cook[1], **R O Dendy**[1,2] **and S C Chapman**[1,3]

[1] Centre for Fusion Space and Astrophysics, Department of Physics, Warwick University, Coventry CV4 7AL, UK
[2] EURATOM/CCFE Fusion Association, Culham Science Centre, Abingdon, Oxfordshire OX14 3DB, UK
[3] Department of Mathematics and Statistics, University of Tromsø, N-9037 Tromsø, Norway

Received 4 December 2012, in final form 20 March 2013
Published 29 April 2013
Online at stacks.iop.org/PPCF/55/065003

Abstract
Ion cyclotron emission (ICE) is the only collective radiative instability, driven by confined fusion-born alpha-particles, observed from deuterium–tritium (DT) plasmas in both JET and TFTR. Using first principles particle-in-cell simulations of the magnetoacoustic cyclotron instability (MCI), we elucidate some of the fully kinetic nonlinear processes that may underlie observations of ICE from fusion products in these large tokamaks. We find that the MCI is intrinsically self-limiting on very fast timescales, which may help explain the observed correlation between linear theory and observed ICE intensity. The simulations elaborate the nature of the excited electric and magnetic fluctuations, from first principles, confirming the dominant role of fast Alfvénic and electrostatic components which is assumed ab initio in analytical treatments.

(Some figures may appear in colour only in the online journal)

1. Introduction

Heat supplied by fusion-born alpha-particles colliding with thermal electrons is essential for sustained nuclear burning in magnetically confined deuterium-tritium fusion plasmas. This heating was measured in TFTR [1] and in JET [2], and will be crucial for ITER [3–5]. It rests on fusion-born alpha-particles delivering almost all of their initial energy, 3.5 MeV, to the thermal electrons on a collisional timescale of $\sim$0.5 s. However this collisional heating can be pre-empted by fast collective instabilities driven by the alpha-particle population, involving the excitation of electric and magnetic oscillations in the plasma at wave-particle resonance [3–5]. A prime instance of such an instability is ion cyclotron emission (ICE). This is the first collective radiative instability driven by confined fusion-born ions that was observed in a tokamak [6, 7], and it was the only such instability, driven by confined fusion-born alpha-particles, that was observed from deuterium–tritium (DT) plasmas in both JET and TFTR [8–12]. ICE was first detected from injected beam ions [13–15] in tokamaks, and is increasingly ubiquitous and topical, having been detected recently in the large tokamaks JT-60U [18] and ASDEX-U [19]. In DIII-D, ICE has recently been used as a diagnostic [20] of energetic ions selectively ejected from the core plasma by fishbone oscillations. Originating in the outer plasma, the ICE from DIII-D is thought to be magnetoacoustic waves excited by the anisotropic bump-on-tail velocity distribution function caused by the fishbone-induced losses. Similar effects have also been observed from regions of Earth's magnetosphere where minority populations of energetic ions with ring-type velocity distributions are present [16, 17].

The range and diversity of observed ICE phenomenology thus continues to grow. In the present paper, we focus on interpreting measurements of ICE driven by confined fusion products in JET and TFTR. In these large tokamaks, ICE is strongly suprathermal and narrowly peaked at the frequencies of sequential ion cyclotron harmonics as evaluated at the outer mid-plane edge, see for example the spectrum from the

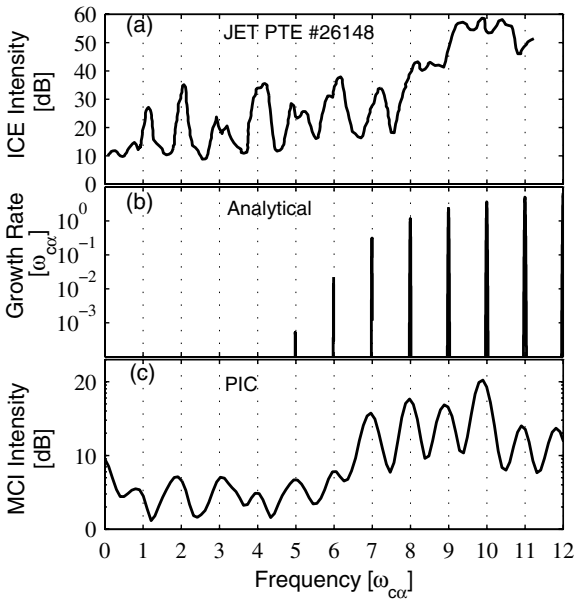

Figure 1. Experimental, analytical and computational spectra. (*a*) Upper panel: measured ICE intensity from JET PTE pulse 26148 (reproduced from figure 3 of [8], with $\omega_{c\alpha}/2\pi = 17$ MHz). (*b*) Middle panel: the linear growth rate of the MCI calculated from equation (8) of [11]. (*c*) Lower panel: the intensity of waves in B_z computed in a PIC simulation of a relaxing 3.5 MeV ring distribution of minority alpha-particles with a number density ratio, $n_\alpha/n_\mathrm{D} = 10^{-3}$. Frequency is plotted in units of the alpha-particle cyclotron frequency $\omega_{c\alpha}$.

preliminary tritium experiment (PTE) in JET, figure 1(*a*). ICE from DT plasmas was detected using a heating antenna in receiver mode in JET and using probes in TFTR. This provides a potentially important diagnostic in burning plasmas since the measured intensity of ICE spectral peaks is empirically found to scale linearly with measured fusion reactivity [8, 11]. The linear theory of ICE has been developed in terms of the magnetoacoustic cyclotron instability (MCI) [21], extended [9, 11, 22] to JET and TFTR regimes, and generalized to more realistic magnetic field geometry [23, 24]. The MCI involves resonance between: the fast Alfvén wave of characteristic speed V_A, which is an extension of the magnetoacoustic mode; cyclotron harmonic waves supported by the background thermal plasma and in some cases by the energetic ions; and a subset of centrally born trapped fusion product ions, close to the trapped-passing boundary in velocity space, whose drift orbits in JET and TFTR make large radial excursions to the outer mid-plane edge (see figures 14–17 in [8] and figures 2 and 3 in [9]). In figure 1(*b*) we plot the analytical linear growth rate of the MCI in a simple, locally uniform, approximation as formulated in equation (8) of [11]. The peaks in analytical linear growth rate can be seen to agree surprisingly well with both the peaks in RF intensity at ion cyclotron harmonics and the trend of increasing intensity with harmonic number shown in figure 1(*a*). This close correspondence is also seen e.g. in figure 6 of [11]. These results suggest that some process operates to constrain the ICE amplitude such that it scales with the linear growth rate. This poses the question, what is the amplitude limiting process or processes, and will they operate in future burning plasmas such as ITER? Here we address this question by performing the first fully self-consistent nonlinear kinetic simulations of the MCI. Our objective is to identify the extent to which the observed properties of ICE from fusion products may be intrinsic to the basic character of the MCI. Our treatment necessarily omits more detailed spatial effects, such as the consequences of toroidal geometry, and physics unfolding on timescales that are long compared to the MCI growth time, for example collisional slowing-down of fast ions.

2. Model simulations

We use a first principles particle-in-cell (PIC) [25, 26] code [27, 28], which self-consistently evolves particle dynamics and the electromagnetic fields using the full Maxwell's equations and the relativistic Lorentz force law:

$$\nabla\cdot\boldsymbol{J} = -\frac{\partial\rho}{\partial t}, \qquad \nabla\cdot\boldsymbol{B} = 0,$$
$$\nabla\times\boldsymbol{E} = -\frac{\partial\boldsymbol{B}}{\partial t}, \qquad \nabla\times\boldsymbol{B} = \mu_0\boldsymbol{J} + \mu_0\epsilon_0\frac{\partial\boldsymbol{E}}{\partial t},$$
$$\frac{\mathrm{d}\boldsymbol{p}}{\mathrm{d}t} = q(\boldsymbol{E}+\boldsymbol{v}\times\boldsymbol{B}). \tag{1}$$

Here $\boldsymbol{J}$, $\boldsymbol{E}$ and $\boldsymbol{B}$ are the current, electric field and magnetic field vectors; ρ is the charge density; and q, $\boldsymbol{v}$ and $\boldsymbol{p}$ are the particle charge, velocity and relativistically correct momentum respectively. The particular numerical integration scheme of the Vlasov–Maxwell system of equations can be found in [26].

This mathematical description captures fast electromagnetic waves and Landau and cyclotron wave-particle resonances. Finite temperature effects and the temporal evolution of the particle distributions are incorporated, as is the full electromagnetic field. In these simulations, the vector fields $\boldsymbol{E}(x,t)$ and $\boldsymbol{B}(x,t)$ are updated on a one-dimensional spatial grid alongside the four dimensional phase space distribution function $f(\boldsymbol{v},x,t)$ of each species. We apply periodic boundary conditions on a large spatial domain discretized into 2048 grid cells, such that the wavenumber space of the instability is adequately resolved. We use 100 particles per cell and a quiet start method from [25]. We represent the initial energetic ion distribution as a mono-energetic ring in velocity space with $v_\parallel = 0$, where particles are quasi-uniformly distributed in gyrophase.

For comparison with observations of ICE from the outer mid-plane of JET [8], we perform simulations with the direction of variation x, and hence the propagation direction of excited waves, exactly perpendicular to $\boldsymbol{B}$. We adopt a ring distribution of 3.5 MeV alpha-particles where $f(v) = (2\pi u)^{-1}\delta(v_\perp - u)$. A more realistic distribution function for applications to ICE [9, 11, 22] would include a non-zero parallel drift velocity, and a small but finite thermal spread. However in this initial study, we neglect these features. Bulk plasma parameters approximate the outer mid-plane edge conditions of the JET PTE pulse 26148. The electron density of $10^{19}\,\mathrm{m}^{-3}$ and the initial applied magnetic field of 2.1 T render the alpha-particles in the initial ring distribution super-Alfvénic, $u > V_\mathrm{A}$. The single spatial direction plays the role of the radial direction in a small region on the outer mid-plane edge of a large tokamak so that waves propagate perpendicular to the magnetic field. The simulations thus

map to the experimental configuration for ICE measurement in JET [8, 10], where an ICRH antenna close to the plasma at the outboard mid plane was used in receiver mode to detect perpendicular propagating waves excited nearby. The smallest ratio of minority alpha-particle number density to that of deuterons that we simulate is 10^{-3}. This value is ∼50 times larger than in JET, and is the lowest value compatible with an acceptable signal-to-noise ratio across the full range of frequencies for which ion cyclotronic features are observed in the JET ICE spectrum. The bulk deuterons and electrons have initial temperatures of 1keV, and the initial densities of all species are uniform in space.

We now compare the output of this simulation, figure 1(*c*), with both linear analytical theory, figure 1(*b*) [11] and experimental measurements, figure 1(*a*). The plasma and energetic particle parameters used to generate figure 1(*b*) are identical to those in the simulations. The width of the ring in velocity space, the quantity v_r in [11], is taken to be that found at $t \simeq 4\tau_{c\alpha}$ in the simulation, where $\tau_{c\alpha} = 2\pi/\omega_{c\alpha}$ is the alpha-particle cyclotron period. The angle between the magnetic field and the direction of propagation is 89°, in order to resolve the narrow range of unstable frequencies that cannot be easily reproduced for an angle of 90°. In the PIC simulations that give rise to the frequency spectrum, figure 1(*c*), of the B_z component of the excited magnetic field shows power at successive alpha-particle cyclotron harmonics. This signal power is $\propto B_z^2$ and is calculated by integrating over the $k > 0$ region of the spatio-temporal fast Fourier transform (FFT) of the $B_z(x,t)$ field signal. This captures the forwards travelling waves only and encompasses the whole simulation domain and the linear phase of the instability in time. The forwards travelling waves correspond to those propagating radially outwards in the tokamak perpendicular to the magnetic field. All three spectra show peaks at ion cyclotron harmonics and the same trend of intensity increasing with harmonic number. The extent to which the simulation spectrum agrees with the experimental one suggests that the signal is dominated by waves excited in the linear regime.

This close correspondence between the measured ICE signal intensity in JET, the linear growth rate of the MCI, and the field amplitude in our PIC simulation provides immediate physical insights into why the measured signal intensity correlates with linear growth rate. In our simulations, the ring distribution relaxes due to the instability and is not replenished by fresh energetic ions. Figure 2 indicates how the instability drive is rapidly reduced in these circumstances. The simulation results in figure 1(*c*) are in good agreement with what is seen in the JET experiments, figure 1(*a*), suggesting that the experiments were also in this regime. We emphasize that this self-limitation of the amplitude of the excited fields is intrinsic to the physics of the MCI as it evolves through the linear regime on ion cyclotron timescales. The close correspondence with linear theory is also seen in simulations for ratios of alpha-particle to deuteron number densities of 10^{-2} and $10^{-2.5}$, and is studied further below, see figure 3(*b*).

The width of the cyclotron harmonic peaks and height in figure 1(*c*) is calculated by integrating over the wavenumber space of the B_z field in the PIC simulations. This integrated signal includes a contribution to the intensity by the excited dispersive ion-Bernstein waves, which sweep in frequency from one ion cyclotron harmonic to the next; see the spectral region $0 < \omega/\omega_{c\alpha} < 5$ and $5 < kV_A/\omega_{c\alpha} < 40$ in figure 3(*d*).

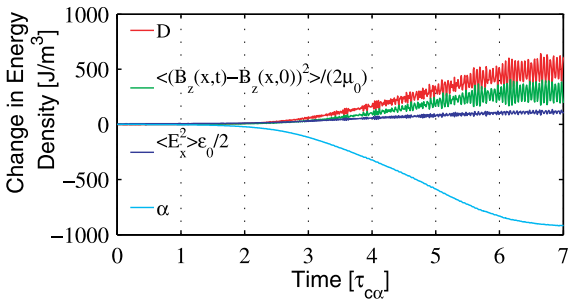

Figure 2. Time evolution of particle and field energy. Spatially averaged temporal evolution of the change in kinetic energy density of the alpha-particles (bottom trace) and deuterons (top trace); and the change in energy density of the dominant vector components of the excited electric and magnetic fields: the electrostatic field $\langle E_x^2\rangle\epsilon_0/2$ (second trace from bottom), and the oscillatory part of the magnetic field $\langle(B_z(x,t) - B_z(x,0))^2\rangle/(2\mu_0)$ (second trace from top). Time is plotted in units of the alpha particle cyclotron period $\tau_{c\alpha} = 2\pi/\omega_{c\alpha}$.

Figure 2 plots the time variation of the spatially averaged kinetic energy of the alpha-particles and of the deuterons, alongside that of the most strongly perturbed field component energy densities. We see that the linear phase of the instability takes place over the first ∼5–6 alpha-particle cyclotron periods, after which the free energy of the initial ring distribution of alpha-particles has become exhausted and a steady state wavefield is established. ICE was detected by an RF antenna (electromagnetic) in JET and by probes (electrostatic) in TFTR. Figure 2 shows that the excited waves primarily generate an oscillatory part of B_z, and also perturb the electrostatic component of the electric field E_x. These data support the assumptions made in the analytical theory of the MCI, which relies on a wave with hybrid character; it is partly fast Alfvénic, implying a fast magnetoacoustic electromagnetic polarization, $\delta\boldsymbol{B} \parallel B_z$; and it is partly cyclotron harmonic and Bernstein in character, implying a significant longitudinal component in δE_x, which is the component aligned with k. The energy density of the alpha-particle population declines by ∼15% during the linear stage of the instability. The majority of this energy is deposited in the collective oscillation of fast Alfvén cyclotron harmonic waves supported by collective motion of the background deuterons, which demonstrates that ICE can operate as a rapid collective means of energy transfer from alpha-particles to bulk fuel ions [30].

3. Electric and magnetic fields

Unlike the linear analytical theory of the MCI, the present self-consistent nonlinear kinetic simulations provide full spatio-temporal electric and magnetic fields and particle distributions, which we now use to diagnose the underlying physics. In figures 3(*a*) and (*d*) we plot the frequency-wavenumber amplitude spectrum of the B_z field component, given by its

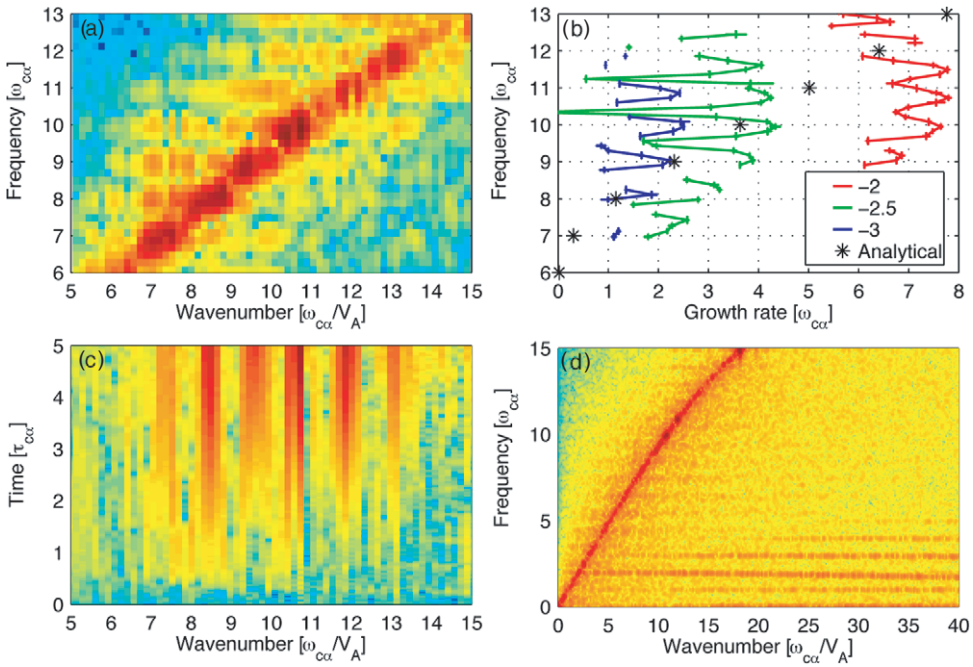

Figure 3. Simultaneous excitation of multiple ion cyclotron harmonics. (*a*) Shading indicates $\log_{10}$ of the amplitude of the oscillatory part of the B_z field component in frequency-wavenumber space, during the linear phase of the instability. (*b*) The real frequency of the most powerful excited modes plotted against their growth rate inferred from the PIC simulations, for three values of the ratio of alpha-particle number density to the number density of deuterons, $\log_{10}(n_\alpha/n_\mathrm{D}) = -2, -2.5, -3$. Asterisks indicate the peaks in the analytical linear growth rate plotted in figure 1(*b*). (*c*) Shading indicates the amplitude of the oscillatory part of the B_z field component as a function of time and wavenumber. (*d*) An expanded view of the excited fast Alfvén mode with resonant cyclotron harmonics and electromagnetic ion-Bernstein modes. The range in wavenumber of data shown in panels (*a*) and (*c*) is identical; and the range in frequency of data shown in panels (*a*) and (*b*) is identical. Frequencies and growth rates are plotted in units of the alpha-particle cyclotron frequency, wavenumbers in units of the alpha-particle cyclotron frequency divided by the Alfvén speed, and time is normalized to the alpha-particle cyclotron period $\tau_{c\alpha} = 2\pi/\omega_{c\alpha}$. The two left panels and the lower right panel show data for $n_\alpha/n_\mathrm{D} = 10^{-3}$.

two-dimensional spatio-temporal FFT. The amplitude of the fast Alfvén branch is corrugated, with peaks in intensity located near the alpha-particle cyclotron harmonics. The Alfvén branch is intersected by approximately horizontal Bernstein cyclotron harmonic modes that are excited by the energetic alpha-particles and also supported by the bulk deuterons. The fine structure of these modes is shown in figure 3(*a*), which shows that there is a strong perturbation to the B_z field component near $6 \leqslant \omega/\omega_{c\alpha} \leqslant 11$ and $6 \leqslant kV_\mathrm{A}/\omega_{c\alpha} \leqslant 12$. The most powerful mode in this spectral region is where this cyclotron harmonic intersects the Alfvén branch at $\omega/\omega_{c\alpha} \simeq 10$ and $kV_\mathrm{A}/\omega_{c\alpha} \simeq 10.5$. This can also be seen in figure 1(*c*). Figure 3(*c*) shows the temporal evolution of the signal shown in figure 3(*a*) for the same range of wavenumbers. From these data we have calculated the linear growth rates of the most powerful modes on the Alfvén branch as a function of wavenumber, and hence frequency. These inferred linear growth rates are plotted in figure 3(*b*) for simulations having number density ratios $\log_{10}(n_\alpha/n_\mathrm{D}) = -2, -2.5, -3$. Cyclotron harmonic peaks are well defined in all three cases. The peaks in the analytical linear growth rate for $n_\alpha/n_\mathrm{D} = 10^{-3}$ (see figure 1(*b*)) are marked by asterisks on figure 3(*b*). We find that the growth rate of the sum of all modes scales with this ratio to the power of 0.5 ± 0.1.

Figure 4(*a*) plots the energy spectra of each component of the electric and magnetic fields excited by the MCI, as a function of wavenumber. These data are calculated by integrating over the $\omega > 0$ region of the 2D FFT of the spatio-temporal field component. The traces thus encompass data from the whole simulation domain in space and the linear phase of the instability in time. Figure 4(*a*) shows that the energy content in the wavenumber region $0 \leqslant kV_\mathrm{A}/\omega_{c\alpha} \leqslant 10$, corresponding to the first few fast Alfvén-cyclotron harmonics of ICE, shown in figures 1 and 2, is dominated by fluctuations in B_z. At high k, the energy spectra of the electric and magnetic fields are dominated by the E_x and B_z components. This reflects the energy in the alpha-particle-driven Bernstein cyclotron harmonic modes, which can be seen in the spectral region $1 < \omega/\omega_{c\alpha} < 4, 10 < kV_\mathrm{A}/\omega_{c\alpha} < 40$ of figure 3. Figure 4(*b*) shows a snapshot in time of the quantities $(\epsilon_0/2)^{1/2}E_x$ and $(2\mu_0)^{-1/2}B_z$ in configuration space. This plot shows that the large amplitude magnetic waveform ($\delta B_z/B_z(t = 0) \simeq 2\%$) is $\sim\pi/2$ out of phase with that of the E_x field. Figure 4(*c*) plots the distribution of alpha-particles with respect to position and gyrophase angle at $t \simeq 3.1\tau_{c\alpha}$, with colour representing energy in MeV. By this time, the initially narrow velocity space distribution of alpha-particles has broadened to a full-width at half-maximum of order $0.1V_\mathrm{A}$, and there has been substantial net energy loss from the population as a whole, as shown in figure 2. The degree of structure visible in figure 4(*c*) reflects the phase space structure of simultaneous resonant wave-particle interaction at multiple ion cyclotron harmonics. One may compare the relative simplicity of the gyrophase-spatial plots for a scenario

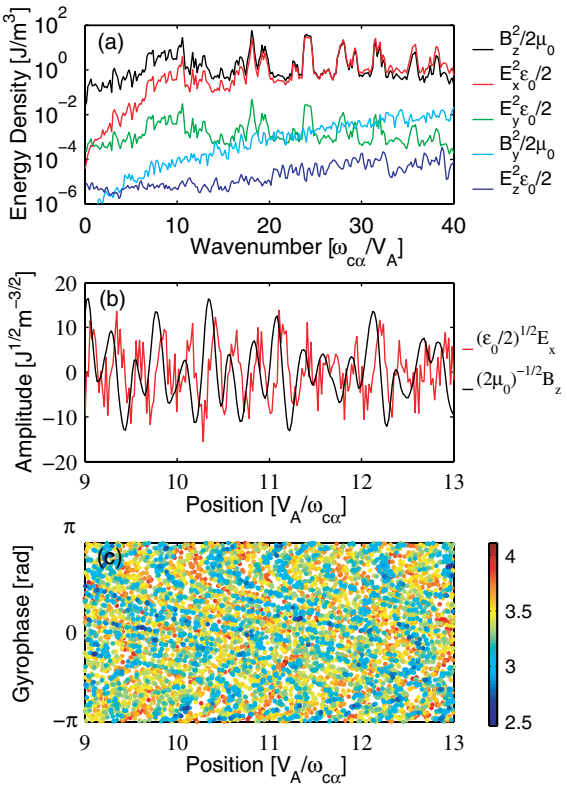

Figure 4. Spatial organization of field components and particle phase space. Upper panel: energy spectrum, as a function of wavenumber, of the oscillatory part of each component of the EM field. The spectra show waves with $k > 0$ and are constructed by integrating over all frequencies during the linear phase of the instability in time. Middle panel: normalized E_x and oscillatory B_z components of the EM field as functions of position at $t \simeq 3.1\tau_{c\alpha}$. Lower panel: shading indicates the energy in MeV of alpha-particles in gyrophase-position space at $t \simeq 3.1\tau_{c\alpha}$. Here gyrophase is $\arctan(v_y/v_x)$. Position is plotted in units of the ratio of the Alfvén speed to the alpha-particle cyclotron frequency.

where a drifting ring-beam population excites a very small number of modes, figure 3 of [29]. In the present case, the high density of resonances in phase space, and their associated self-consistent dispersion of particles in phase space, limits the growth of coherent perturbative structure in both the particle phase space and the wavefield for any given wavemode. ICE is distinctive partly because the value of the linear growth rate is comparable across multiple harmonics. Our simulations show this, in addition, the phase space separation of these resonances is sufficiently small so that overlap of perturbative structures occurs. Consequently, the coherent wave–particle resonances break down before the field amplitudes can progress much beyond the linear regime.

4. Conclusions

Using first principles fully kinetic nonlinear simulations, we have elucidated the plasma physics processes which arise in the magnetoacoustic cyclotron instability. This instability is of particular interest for magnetic confinement fusion, because it appears to underlie observations [6–12, 15, 18, 19] of ICE from energetic ions in large tokamaks. These simulations help explain the correlation between linear analytical MCI growth rate and observed ICE intensity. The simulations elaborate the nature of the excited electric and magnetic fluctuations, confirming the dominant role of fast Alvénic and electrostatic components which is assumed ab initio in analytical treatments.

Our simulations represent the simplest case, in which a ring distribution of fusion-born ions is introduced as an initial condition, and no particle source or loss terms are included. This population then relaxes due to collisionless instability as the simulation progresses. There is competition between wave growth, driven by the free energy of the ring distribution of fusion-born alpha-particles, and the associated self-consistent velocity space dispersion. Underpinning our model is the explicit assumption that this relaxation will be fast compared with other processes affecting the ion distribution, which are accordingly neglected in this simulation. This assumption is then justified retrospectively by the success of the model in reproducing the experimental observations.

Acknowledgments

The authors thank N J Fisch and K G McClements for useful discussions. We acknowledge the EPSRC for support. This project used the EPOCH code developed under EPSRC grant EP/G054950/1. This work was part-funded by the RCUK Energy Programme under grant EP/I501045 and the European Communities under the contract of Association between EURATOM and CCFE. The views and opinions expressed herein do not necessarily reflect those of the European Commission.

5. References

[1] Taylor G, Strachan J D, Budny R V and Ernst D R 1996 *Phys. Rev. Lett.* **76** 2722
[2] Thomas P R *et al* 1998 *Phys. Rev. Lett.* **80** 5548
[3] ITER Physics Experiment Group 1999 *Nucl. Fusion* **39** 2471
[4] Heidbrink W W 2002 *Phys. Plasmas* **9** 2113
[5] Fasoli A *et al* 2007 *Nucl. Fusion* **47** S264
[6] Cottrell G A and Dendy R O 1988 *Phys. Rev. Lett.* **60** 33
[7] Schild P, Cottrell G A and Dendy R O 1989 *Nucl. Fusion* **29** 834
[8] Cottrell G A *et al* 1993 *Nucl. Fusion* **33** 1365
[9] Cauffman S, Majeski R, McClements K G and Dendy R O 1995 *Nucl. Fusion* **35** 1597
[10] Dendy R O *et al* 1995 *Nucl. Fusion* **35** 1733
[11] McClements K G, Dendy R O, Lashmore-Davies C N, Cottrell G A, Cauffman S and Majeski R 1996 *Phys. Plasmas* **3** 543
[12] McClements K G, Hunt C, Dendy R O and Cottrell G A 1999 *Phys. Rev. Lett.* **82** 2099
[13] Heidbrink W W and Sadler G J 1994 *Nucl. Fusion* **34** 535
[14] Dendy R O, McClements K G, Lashmore-Davies C N, Majeski R and Cauffman S 1994 *Phys. Plasmas* **1** 3407
[15] Cottrell G A 2000 *Phys. Rev. Lett.* **84** 2397
[16] McClements K G and Dendy R O 1993 *J. Geophys. Res.* **98** A 11689
[17] McClements K G, Dendy R O and Lashmore-Davies C N 1994 *J. Geophys. Res.* **99** A23685

[18] Ichimura M, Higaki H, Kakimoto S, Yamaguchi Y, Nemoto K, Katano M, Ishikawa M, Moriyama S and Suzuki T 2008 *Nucl. Fusion* **48** 035012
[19] D'Inca R, Garcia-Munoz M, Tardini G and Noterdaeme J-M 2011 *Proc. 38th EPS Conf. on Plasma Physics (Strasbourg, France)* P1.053
[20] Heidbrink W W *et al* 2011 *Plasma Phys. Control. Fusion.* **53** 085028
[21] Belikov V S and Kolesnichenko Ya I 1976 *Sov. Phys. Tech. Phys.* **20** 1146
[22] Dendy R O, Lashmore-Davies C N, McClements K G and Cottrell G A 1994 *Phys. Plasmas* **1** 1918
[23] Gorelenkov N N and Cheng C Z 1995 *Phys. Plasmas* **2** 1961
[24] Fülöp T, Lisak M, Kolesnichenko Ya I and Anderson D 2000 *Phys. Plasmas* **7** 1479
[25] Sydora R D 1999 *J. Comput. Appl. Math.* **109** 243
[26] Bonitz M, Bertsch G, Filinov V S and Ruhl H 2004 *Introduction to Computational Methods in Many Body Physics* (Cambridge: Cambridge University Press)
[27] Cook J W S, Chapman S C and Dendy R O 2010 *Phys. Rev. Lett.* **105** 255003
[28] Cook J W S, Chapman S C, Dendy R O and Brady C S 2011 *Plasma Phys. Control. Fusion* **53** 065006
[29] Cook J W S, Dendy R O and Chapman S C 2011 *Plasma Phys. Control. Fusion* **53** 074019
[30] Fisch N J and Rax J-M 1992 *Phys. Rev. Lett.* **69** 612